# Ordering kinetics of block copolymers directed by periodic two-dimensional rectangular fields

Weihua Li,[1,a)] Nan Xie,[1] Feng Qiu,[1] Yuliang Yang,[1] and An-Chang Shi[2]
[1]*The Key Laboratory of Molecular Engineering of Polymers, Ministry of Education, China, Department of Macromolecular Science, Fudan University, Shanghai 200433, China*
[2]*Department of Physics and Astronomy, McMaster University, Hamilton, Ontario L8S 4M1, Canada*

(Received 10 January 2011; accepted 7 March 2011; published online 8 April 2011)

The ordering kinetics of directed assembly of cylinder-forming diblock copolymers is investigated by cell dynamics simulation of the time-dependent Ginzburg–Landau theory. The directing field, mimicking chemically or topologically patterned surfaces, is composed of a rectangular array of potential wells which are attractive to the minority blocks. The period of the templating fields is commensurate with the hexagonal lattice of the block copolymer domains. The ordering kinetics is described by the time evolution of the defect concentration, which reveals that the rectangular field of [1 m] for a given density multiplication has the best directing effect, and the reversed case of [m 1] has the worst. Compared with a hexagonal directing field, the rectangular field provides a better directing efficiency for a fixed high density multiplication. The difference of the directing effect can be understood by analyzing the ordering mechanisms in the two types of directing fields. The study reveals that the rectangular pattern is an alternative candidate to direct block copolymer assembly toward large-scale ordered domains. © *2011 American Institute of Physics*. [doi:10.1063/1.3572266]

## I. INTRODUCTION

Block copolymer (BCP) lithography, by taking advantage of the BCP ability to self-assemble into ordered microstructures, has received abiding interest by researchers in chemistry, physics, materials science, and nanotechnology. The BCP lithography technique has the potential to produce high-density multiplication of periodic patterns by directed assembly of BCPs on patterned substrates. Therefore BCP lithography is viewed as a promising technique to overcome the intrinsic limitation of standard photolithography, and to decrease the cost of e-beam lithography of sub-30-nm patterns which is required for improved data storage and computing speed in semiconductor technologies and other advanced materials.[1–5] Furthermore BCPs, via the change of their architectures, can self-assemble into a variety of ordered structures.[6] This feature enriches the application of BCP lithography.

For the purpose of practical application in high-performance functional materials, it is desirable that the BCP patterns possess long-range order and uniform domain shapes which can hardly be achieved by uncontrolled BCP self-assembly in bulk. The reason is that the equilibrium structure competes with a multitude of metastable morphologies that have a minimally higher free energy, as well as the unavoidable presence of defects. Typical differences in free energy between a stable morphology and alternative structure are on the order of $10^{-3}k_BT$ per macromolecule (where $k_BT$ denotes the thermal energy scale). This small free energy difference makes it hard to obtain long-range order in a free-standing system. At the same time, it provides the opportunity of using external interactions to stabilize metastable morphologies, particularly in thin films. A number of schemes, including shear,[7] electric fields,[2] thermal gradients,[8,9] solvent annealing,[10] flow,[11] graphoepitaxy,[12–14] and chemical prepatterning,[15,16] have been proposed to improve the ordering of BCP domains. Among these different possibilities, the graphoepitaxy based on prepatterned templates is one of the most used techniques to form large-scale perfectly ordered patterns in thin films. Recently significant advances have been achieved in the manufacturing of large-scale ordered patterns by means of directed assembly of BCPs on patterned substrates.[17–21] Ruiz *et al.* used a sparse chemical patterns to direct BCPs to form a fourfold density multiplication of perfectly ordered hexagonal cylinders.[17] With substrates decorated by hexagonally arranged nanoposts, Bita *et al.* realized another effective graphoepitaxial method to direct the BCP assembly of thin films,[18] achieving up to about 21-fold density multiplication. In addition, great efforts have been dedicated to fabricate many complex patterns to expand the applications of BCP lithography.[22–26]

To obtain perfectly ordered hexagonal patterns (cylinder or single-layer sphere) in thin films, a sparse hexagonal template is often used to direct the BCP assembly. In our previous work, the ordering kinetics of the BCP assembly directed by periodic two-dimensional (2D) hexagonal fields was investigated by cell dynamic simulation (CDS) of the time-dependent Ginzburg–Landau (TDGL) theory. Our results reveal that the ordering effect is efficient when the length ratio of $L_s/L_0$ is an integer which is not larger than four. In this case the defect concentration decreases exponentially with time. Here the two feature lengths $L_s$ and $L_0$ are the distance between the potential wells and the cylinder-to-cylinder distance of the bulk BCP phase, respectively. When $L_s/L_0 = 6$, the field does not have an obvious directing effect on the ordering behavior and the evolution of defect concentration with time is similar as that in the bulk. The case of $L_s/L_0 = 5$ is

a)Author to whom correspondence should be addressed. Electronic mail: weihuali@fudan.edu.cn.

 

intermediate between those of $L_s/L_0 = 4$ and 6. The evolution of defect concentration follows a multistep power law instead of the exponential-decay behavior, but the absolute value of power-law coefficient increases with time, which is opposite to the case of $L_s/L_0 = 6$. This suggests that the directing field still has significant effect. Therefore it is concluded that the highest density multiplication predicted from our simulations is not larger than 25-fold with the hexagonal array of periodic 2D fields. This conclusion is well consistent with available experimental observations. In experimental cases of chemically prepatterned surfaces, the film thickness plays a crucial role to form perpendicularly standing cylinders on substrates (usually chosen as around $1.6L_0$).[19,20,27] By carefully controlling the film thickness, fourfold density multiplication can be achieved by means of chemically patterned templates,[17,19,27] and even a multiplication as high as ninefold has been claimed.[20] Higher multiplication has not been reported by this technique, but by an alternative strategy, i.e., templates prepatterned by hexagonal array of nanoposts to direct the formation of single-layer spheres in thin films.[18] It is reported that the multiplication is as high as about 21-fold. Compared to chemical-pattern surfaces, the array of posts has a 3D directing effect not only on the 2D surface, but also along the normal direction of the films.

In another word, the hexagonal field pattern is replaced by another field with different symmetry, such as rectangular potential wells, what will happen with the directing effect? In the present work, we focus on the investigation of the ordering kinetics of the formation of cylinders by directed BCP assembly on a rectangular array of periodic surface field. To ensure that the rectangular field array is commensurate with the intrinsic hexagonal array of BCP domains, two periods to describe the rectangular 2D field, $L_s^x$ and $L_s^y$, have to be related to $L_0$ by some special algebraic expressions. In what follows we choose $L_s^x = 1\sqrt{3}L_0$ and $L_s^y = \mathrm{m}L_0$ (Fig. 1), and we use [lm] to denote this rectangular array (the square brackets are used to differ from the angular brackets for hexagonal field arrays). The corresponding density multiplication of [l m] (abbreviated as DM), also the ratio between the BCP microdomain number to the field-spot number, is DM = 2 ml. Our previous work suggests that the CDS method of TDGL is highly efficient to give qualitative results on the collective ordering kinetics of the directed assembly by patterned surface, which is useful to judge the relevant directing effect. Therefore the same simulation scheme is applied for the present study. It is assumed that the BCP formed domains are perpendicularly standing cylinders or single-layer spheres in thin film with appropriate film thickness. Thus the system is simplified to be 2D, and the patterned surface is modeled as a periodic 2D fields.

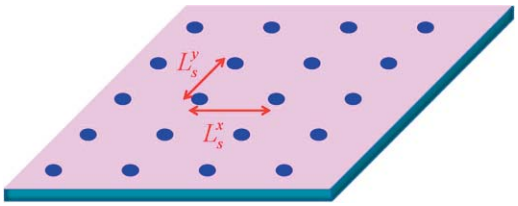


FIG. 1. Schematic plot of periodic rectangular array of potential wells on a substrate. The blue color indicates the regions where the minority block is preferred, and the other regions do not have preference to any block. Each rectangular cell is denoted by two periods of $L_s^x$ and $L_s^y$ on x and y directions, respectively.

## II. MODEL AND THEORY

We consider an incompressible asymmetric AB diblock copolymer with equal monomer size and with polymerization of $N_A$ and $N_B$ for A and B blocks, respectively. Each copolymer has a volume fraction $f = N_A/N$ of the A block, where $N = N_A + N_B$ is the total polymerization of the chain. The local monomer densities of A and B components are denoted as $\phi_A(\mathbf{r})$ and $\phi_B(\mathbf{r})$, respectively. The density difference, $\phi = \phi_A - \phi_B$, is chosen as the order parameter to describe the phase separation and the pattern formation of the diblock copolymer. The model free energy can be written as a functional of $\phi$ which consists of three parts: short-range, long-range, and that of the external field, $H_{\mathrm{ext}}(\mathbf{r})$:[28]

$$F[\phi] = F_S[\phi] + F_L[\phi] + \int d\mathbf{r} H_{\mathrm{ext}}(\mathbf{r})\phi(\mathbf{r}). \tag{1}$$

The short-range part $F_S$ is the usual Ginzburg–Landau free energy and is given by

$$F_S[\phi] = \int d\mathbf{r} \left\{ \frac{D}{2}[\nabla\phi(\mathbf{r})]^2 + W(\phi) \right\}, \tag{2}$$

where $D$ is a positive constant, $W(\phi)$ is the local interaction contribution, and it can be specified by its derivative:

$$\frac{dW(\phi)}{d\phi} = -A\tanh(\phi) + \phi, \tag{3}$$

with $A > 1$. The long-range contribution is originally proposed by Ohta and Kawasaki to alter the phase separation from macroscopic in A/B blends to be microscopic in AB diblock copolymers.[28] The long-range part is expressed as

$$F_L(\phi) = \frac{\alpha}{2} \int d\mathbf{r} \int d\mathbf{r}' G(\mathbf{r} - \mathbf{r}')\delta\phi(\mathbf{r})\delta\phi(\mathbf{r}'), \tag{4}$$

where $\delta\phi(\mathbf{r}) = \phi(\mathbf{r}) - \bar{\phi}$, and $\bar{\phi} = 2f - 1$ is the average value of $\phi(\mathbf{r})$ over the 2D space. In the above expression, $G(\mathbf{r} - \mathbf{r}')$ is a Green function, which can be conveniently specified by

$$-\nabla^2 G(\mathbf{r} - \mathbf{r}') = \delta(\mathbf{r} - \mathbf{r}'). \tag{5}$$

The positive coefficient $\alpha$ in expression (4) is proportional to $1/N^2 f(1-f)$, and is inherent to the block copolymer.[28–30] $H_{\mathrm{ext}}(\mathbf{r})$ in the last term of Eq. (1) is the external field mimicking the chemically patterned surfaces. A potential-well function, similar as that used in our previous work,[21] is used to describe the surface interactions on the two components around the potential well at position $\mathbf{R}_{i,j} = (iL_s^x, jL_s^y)$ ($i = 0, 1, \ldots, n_x^s$ and $j = 0, 1, \ldots, n_y^s$):

$$H_{\mathrm{ext}}(\mathbf{r}) = -\frac{1}{2}V_0 \{ \tanh[(-|\mathbf{r} - \mathbf{R}_{i,j}| + \sigma)/\lambda] + 1 \} \tag{6}$$

for $|\mathbf{r} - \mathbf{R}_{i,j}| < 2\sigma$ and otherwise $H_{\mathrm{ext}}(\mathbf{r}) = 0$. The magnitude $V_0$ indicates the strength of the field, $\sigma$ measures the radial size of each potential well, and $\lambda$ determines the steepness of the potential-well shape. Two integers, $n_x^s$ and $n_y^s$, are

the repeating numbers of the periodic rectangular 2D fields on $x$ and $y$ directions, respectively.

With the above free-energy functional, the dynamics of the density evolution can be described by the Cahn–Hilliard model (Model B):[31]

$$\frac{\partial \phi}{\partial t} = M\nabla^2 \frac{\partial F[\phi]}{\partial \phi} + \eta(\mathbf{r}, t), \tag{7}$$

where $M$ is a phenomenological mobility coefficient, set as $M = 1$, and $\eta(\mathbf{r}, t)$ is a random noise term, with zero average and a second moment of $\langle \eta(\mathbf{r}, t)\eta(\mathbf{r}', t')\rangle = -\eta_0 M\nabla^2\delta(\mathbf{r} - \mathbf{r}')\delta(t - t')$, here $\eta_0$ is the noise strength.

Follow our previous work,[21] we empirically choose these parameters as $D = 0.5$, $f = 0.35$, $A = 1.30$, $\alpha = 0.02$, $V_0 = 0.04$, $\sigma = 0.15L_0$, and $\lambda = 0.5$. The cylinder-to-cylinder distance, $L_0$, for this choice of parameters, has been determined as $L_0 = 9.20$ lattices in our previous work. The values of $n_x^s$ and $n_y^s$ together with those of $L_s^x$ and $L_s^y$ determine the simulated box sizes of $N_x = n_x^s L_s^x$ and $N_y = n_y^s L_s^y$, and therefore they are chosen to ensure that more than $10^4$ BCP domains are formed in each simulated sample. The standard CDS scheme is applied for the Laplacian discretization with periodic boundary conditions imposed on each direction, and the forward Euler algorithm is applied for the time integration with time step of $\Delta t = 1$.

## III. RESULTS AND DISCUSSIONS

From our previous work of hexagonal directing field, it is found that the time evolution of defect concentration is a convenient and efficient quantity to evaluate the directing effect of different field arrays. For denser array of directing hexagonally packed potential wells (⟨30⟩ or ⟨40⟩ with $L_s/L_0 = 3$ and 4, respectively) the defect concentration decays exponentially in time, indicating that large-scale ordered patterns can be obtained by BCP assembly under the direction of the field. For sparser hexagonal field of ⟨50⟩, the time evolution of defect concentration does not decay exponentially, but follows a multistep power law with larger and larger power-law coefficient as time. This is faster than the bulk system. This suggests that ⟨50⟩ still has some directing effect on BCP assembling process, however, it would take a long time to obtain perfect pattern, or to observe small amount of defects in a short time. When the DM is increased further, $DM \geq 6^2$, the directing effect of the field is negligible because the defect evolution is similar as that of bulk system. To evaluate the directing effect of the rectangular field we first computed defect concentration as function of time for various field arrays of two fixed density multiplications of DM = 12 and DM = 16. For both cases, there are four candidate arrays by varying one of the two integers of l and m for fixed DM = 2 lm. The results of DM = 12 and DM = 16 are presented as linear-logarithm plots in Figs. 2(a) and 2(b), respectively. Each set of data is calculated by averaging over 10–16 independent simulated samples. Obviously the directing effect described by defect evolution is dependent on the field array for a given DM. In Fig. 2(a), the defect concentration of [1 6] has the fastest decreasing speed as time, i.e., exponential-decay (highlighted by the green solid line), while that of [6 1] has the slowest

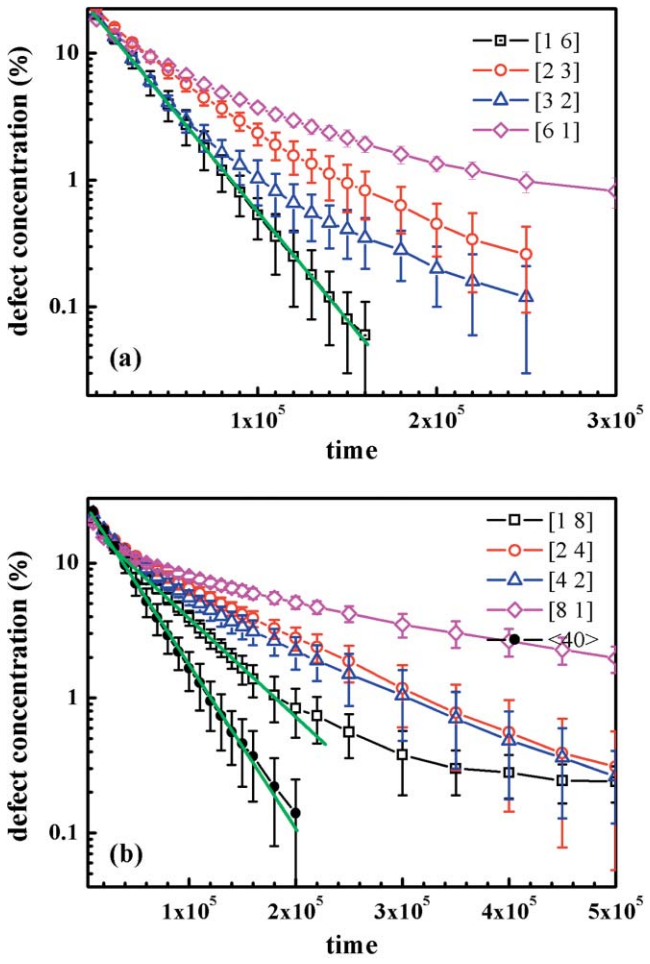


FIG. 2. Defect concentrations of cylinders assembled on patterned templates as function of time. Figures (a) and (b) are results of four rectangular fields for each of density multiplications of 12 and 16, respectively. In (b), the filled symbols denote the results of periodic hexagonal field with the same density multiplication of 16 from Ref. 21.

one. The time evolutions of defects of [2 3] and [3 2] are intermediate between those of [1 6] and [6 1], and that of [2 3] is slower than that of [3 2]. For DM = 16, a similar feature is observed with the defect evolution in Fig. 2(b). The defect evolution of the hexagonal ⟨40⟩-field with the same DM, which is near exponential-decay, is shown as a comparison. It can be seen that the fastest evolution of [1 8] among these rectangular fields is slower than that of ⟨40⟩, and deviates from the exponential relation at the later evolving stage. The simple exponential relation indicates that the correlation of defects is weak, and thus they are annihilated simultaneously. On the other hand, the intermediate defect evolutions between the exponential law and the multistep power law in the bulk indicate that some of defects are connected to form a large grain boundary which takes longer time to be eliminated.

From the two sets of results in Fig. 2, it can be concluded that the type [1 m] field has the best directing effect, and the reverse type of [m 1] has the worst one. To understand the ordering mechanism of BCP microdomains under these different types of field, we first examine the monomer density plots of [1 6] (left column) and [6 1] (right column) at $t = 10^4$

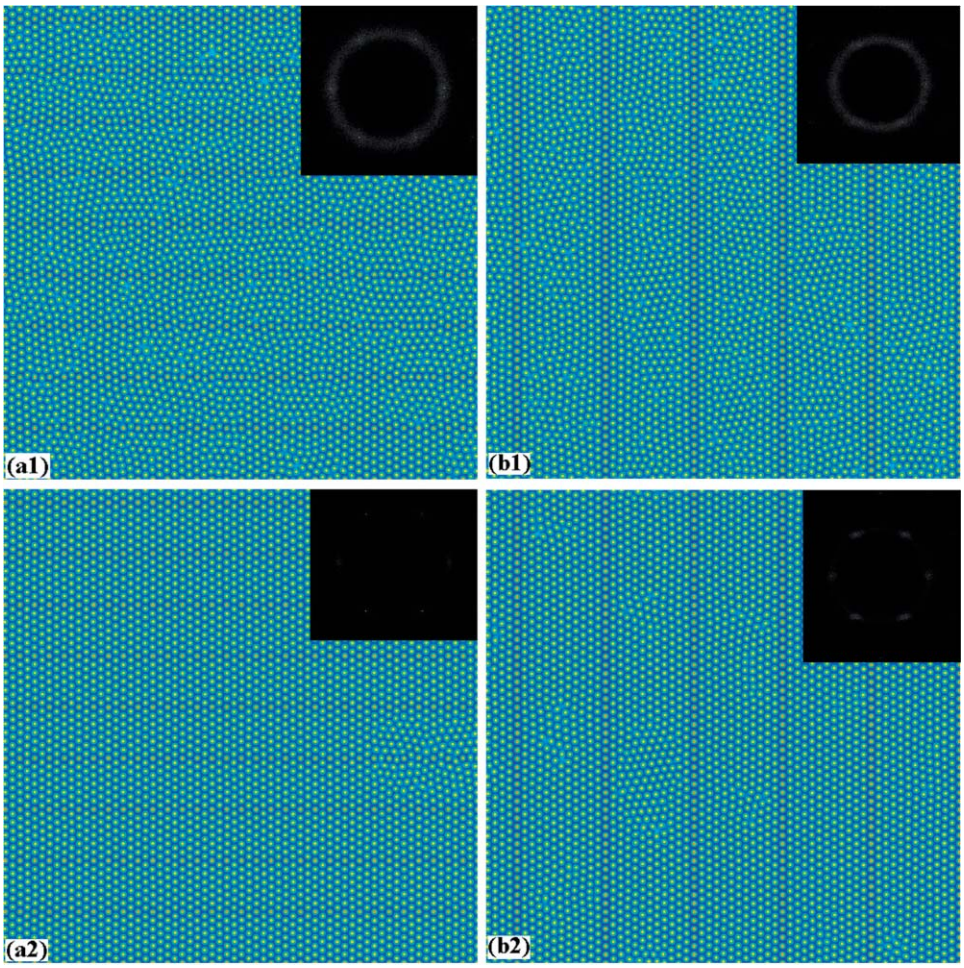


FIG. 3. Monomer density plots of cylinder patterns directed by periodic fields of [1 6] (left column) and [6 1] (right column) at $t = 10^4$ (upper row) and $t = 10^5$ (bottom row). Each figure exhibits a $512^2$ portion of the entire sample. Insets give the Fourier spectrums of the density.

(upper row) and $t = 10^5$ (bottom row) together with their corresponding Fourier spectrums in Fig. 3. The comparison of the Fourier spectrums between [1 6] and [6 1] for $t = 10^5$ indicates unambiguously that the pattern of [1 6] [Fig. 3(a2)] has better degree of order than that of [6 1] [Fig. 3(b2)]. In addition, the corresponding orientation distributions of local domain lattice are calculated and are presented in Fig. 4 (details of calculation are found in Ref. 21), where different colors indicate grains with different lattice orientations. The common feature of [1 m] and [m 1] fields is that their potential-well positions are lined up with distances of $\sqrt{3}L_0$ and $L_0$, or, with row-to-row distance of m$L_0$ and column-to-column distance of m$\sqrt{3}L_0$, respectively. Of course, any type of [l m] can be seen as a set of rows or columns of potential wells. This feature suggests that the potential-well distance in each row or column (denoted as $d_s$) and the row-to-row or column-to-column distance (denoted as $D$) are the two main factors influencing the ordering kinetics. Smaller value of $d_s$ is beneficial to direct layer by layer assembly of cylinders starting from the aligned preformed cylinders on potential wells toward two side directions. For example, it is more obvious to observe the layer by layer formation of ordered cylinders in Fig. 3(b1) than (a1). Furthermore, we can see stripelike patterns along the y-direction in Fig. 4(b1), but not in Fig. 4(a1). However, for a given DM, smaller $d_s$ corresponds to larger $D$. Larger $D$ in Fig. 3(b1) indicates that there is more free space between two neighbor columns to form large grains with mismatched orientation from that of the field array. The defects located on the boundary of those large grains are difficult to be annihilated, particularly those with large angle of mismatched orientation (red grains in orientation distribution maps). At $t = 10^5$, we find that there are more this type of grains in Fig. 4(b1) than 4(a1), resulting in a slower defect annihilation of [6 1] than [1 6].

In order to understand the directing effect of rectangular fields further, we present the orientation distributions of [1 8] (first row) and [8 1] (second row) together with those of the hexagonal field of ⟨40⟩ (third row) at three times of $t = 10^4$, $10^5$ and $2 \times 10^5$ (from left to right) in Fig. 5. The average defect concentrations are $(22.2 \pm 0.7)\%$, $(3.9 \pm 0.5)\%$, and $(0.8 \pm 0.3)\%$ for [1 8], $(19.9 \pm 0.5)\%$, $(8.0 \pm 0.4)\%$, and $(5.1 \pm 0.5)\%$ for [8 1], and $(24.1 \pm 0.7)\%$, $(1.7 \pm 0.5)\%$, and $(0.14 \pm 0.11)\%$, respectively. The comparison of results between [1 8] and [8 1] also supports the conclusion obtained in the above paragraph. In addition, by comparing defect evolutions between the directing fields [1 8] and ⟨40⟩, it is helpful to understand the difference of directing mechanism between rectangular field and hexagonal field. At the early stage

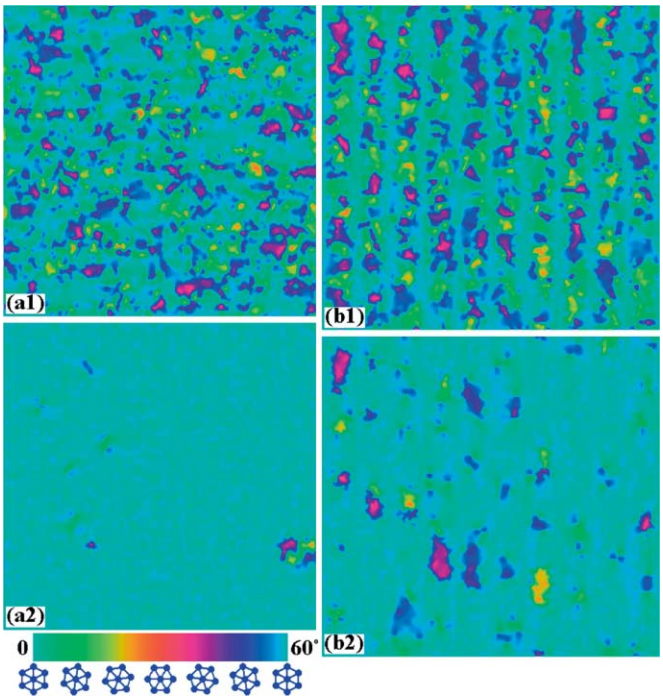


FIG. 4. Distributions of local lattice orientation of the entire block copolymer domains in Fig. 3. The colors of the spectrum indicate the range of lattice orientation from 0 to 60 degrees.

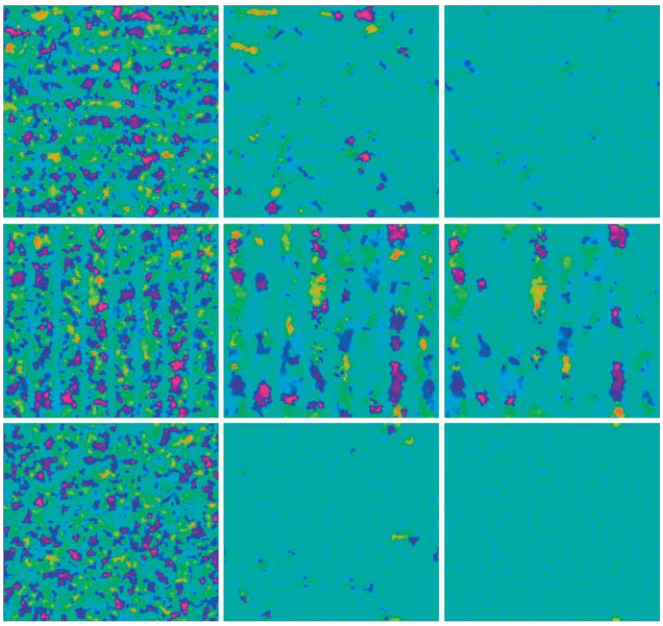

FIG. 5. Orientation distribution plots for the density multiplication of 16. From top to bottom, the periodic field is [1 8], [8 1], and ⟨40⟩, and from left to right, the corresponding time is $t = 10^4$, $10^5$, and $2 \times 10^5$, respectively.

of $t = 10^4$, there is a small difference of orientation distribution between the two settings in that the proportion of relative large grains with large angle of mismatched orientation in [1 8] is higher than that of ⟨40⟩. Compared with the rectangular [1 8]-field, the potential wells in the hexagonal ⟨40⟩-field are more uniformly distributed in the entire sample. As shown in our previous work,[21] the density of potential wells in ⟨40⟩ is high enough such that they tend to stop the formation of large grains with mismatched orientation. In the rectangular [1 8]-field, the nonuniformity of potential wells gives rise to more space free of the directing field, resulting in a larger possibility to form large grains. This point can be seen more clearly from the orientation distributions at $t = 10^5$ where only small amount of large grains are remained. At $t = 2 \times 10^5$, the entire sample with the ⟨40⟩-field is almost perfectly ordered. In contrast, there are still a number of defects remaining in the sample with the [1 8]-field. From the density plots, it is found that most of these defects are in the form of a pair of dislocations, each of which is composed of a pair of fivefold and sevenfold defects. A typical example

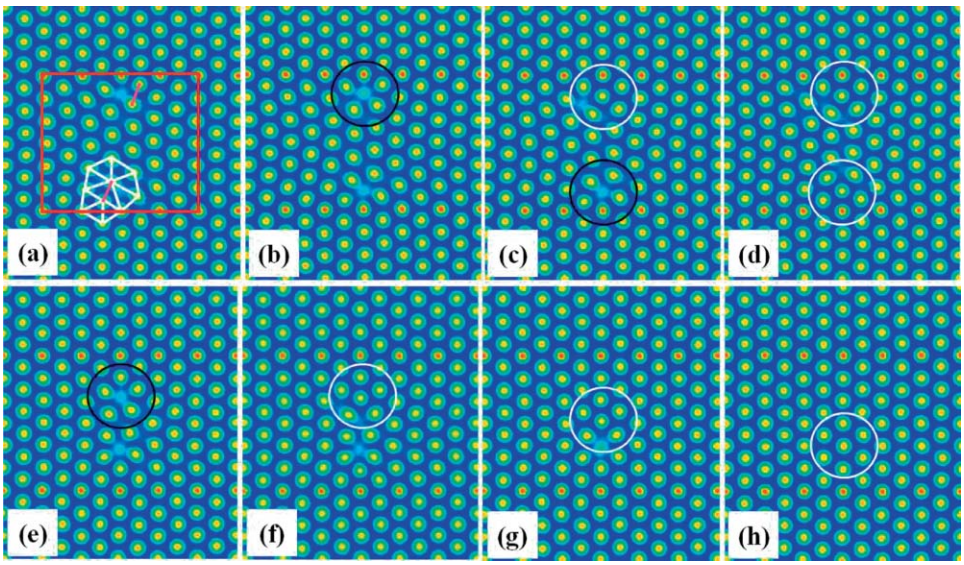


FIG. 6. Small portion of density plots around the locations of a pair of dislocations for the rectangular [1 6]-field. From (a) to (h), the time is $t = 2 \times 10^5$, $2.2 \times 10^5$, $2.4 \times 10^5$, $2.6 \times 10^5$, $3.2 \times 10^5$, $3.4 \times 10^5$, $3.6 \times 10^5$, and $3.8 \times 10^5$, respectively. In (a), the two dislocations are indicated by short color lines, and the Delaunay triangles around the bottom one are plotted. Black and white circles indicate where a new domain is going to appear and where a new domain just comes out, respectively.

of the pair of dislocations is presented as a series of time-evolving density plots for one of running samples with the [1 6]-field in Fig. 6. The time steps of these figures from (a) to (h) are $t = 2 \times 10^5$, $2.2 \times 10^5$, $2.4 \times 10^5$, $2.6 \times 10^5$, $3.2 \times 10^5$, $3.4 \times 10^5$, $3.6 \times 10^5$, and $3.8 \times 10^5$. To focus on the defect evolution, only the area surrounding the defect locations is shown. In Fig. 6(a), the pair of dislocations are indicated by two short color lines, and the Delaunay triangles around one of them are plotted. It is interesting to see that the two dislocations are located near the bottom row and the upper row of potential wells, respectively. Thus their distance is about $5L_0$ which is close but smaller than the row-to-row distance of $6L_0$. This distance is a key factor to determine the life time of these defects. The presence of the periodic field results in that only small portion of lattice orientation of BCP domains is influenced by the small amount of defects (the region inside the red rectangle). Within this region, five BCP domains are needed to annihilate these defects. In Fig. 6(b), these neighboring domains of the dislocations are rearranged to allow the addition of new domains. In the black circle of Fig. 6(b), one new domain is added to form fivefold defect in the white circle of Fig. 6(c). At the same time, the black circle of Fig. 6(c) will allow the addition of another new domain. Defect annihilation proceeds by starting from the two dislocations and propagating toward each other. In this sense, the distance of the dislocations has significant influence on the local ordering time. Therefore, increased line-to-line distance of the potential wells increases the possibility not only to form large grains, but also to produce pairs of dislocations with large distance, and thus slowing down the ordering process.

Although the ordering process of the rectangular [1 8]-field is slower than that of the hexagonal ⟨40⟩-field, it exhibits an exponential relation when $t \leq 2 \times 10^5$ at which the grains with mismatched lattice orientations are diminished [see Fig. 2(b)]. After that, a number of pairs of dislocations with a wide range of life times remain, therefore the ordering process is relative slow. Nevertheless, the rectangular [1 8]-field is still efficient for directing BCP assembly. It is worthy to examine the directing effect of other rectangular fields of the type of [1 m] with larger DM. In Fig. 7, the defect concentrations as function of time for $m = 10$, 12, 14, 16, and 18, together with those of ⟨50⟩ (red line) and ⟨60⟩ (blue line), are shown as double-logarithm plots. At the early stage, the defect concentration approaches a power law with a power coefficient of 1/3 for large values of DM, which is similar as that of bulk system. This suggests that the ordering kinetics is dominated by the formation of large grains, so that the ordering process becomes slow as DM increases. However, it is surprising that the ordering processes of $m = 14$ is faster than that of ⟨50⟩ while the former case has larger DM than the later one. The same feature is also seen from the comparison between the fields of [1 18] and ⟨60⟩, both of which have the same density multiplication of DM = 36. If we view the function of defect concentration as a multistep power law, the coefficient becomes larger and larger, which is different from that of ⟨60⟩. This suggests that it is more likely to obtain well-ordered patterns, or at least, to obtain patterns with lower-density defects, by the direction of [1 18] than by that of ⟨60⟩.

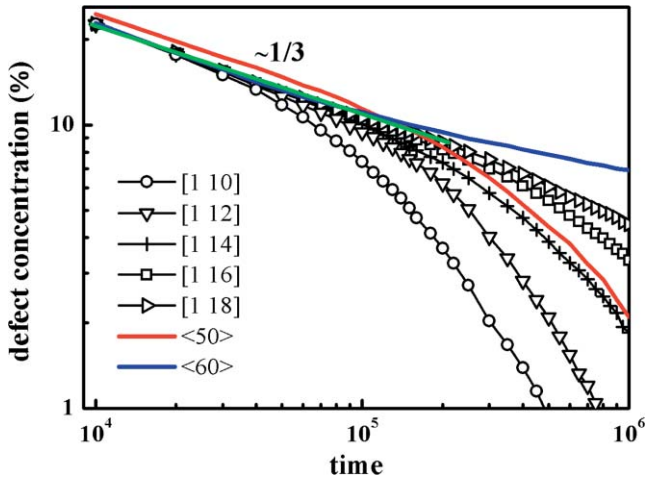


FIG. 7. Time evolution of defect concentrations for the type [1 m] of rectangular field, where m = 10, 12, 14, 16, and 18. The red and blue solid lines are the results of hexagonal field, ⟨50⟩ and ⟨60⟩, respectively. The green solid line indicates the relation of 1/3 power law.

To demonstrate the different ordering mechanisms, we plot both orientation distributions of [1 18] (upper row) and ⟨60⟩ (bottom row) at $t = 10^5$ and $t = 10^6$, respectively, in Fig. 8. Obviously the grains of the sample with the [1 18]-field are much larger than those of the samples with the [1 8]-field, and when $t = 10^5$, these grains have stripelike distribution along the x-direction. The space between two neighboring rows of the potential wells is large enough to form a number of large grains with large mismatched angle of orientation from the field lattice, but the layer-by-layer preformed domains directed by the rows of the potential wells reduces the grain size along the normal direction of these

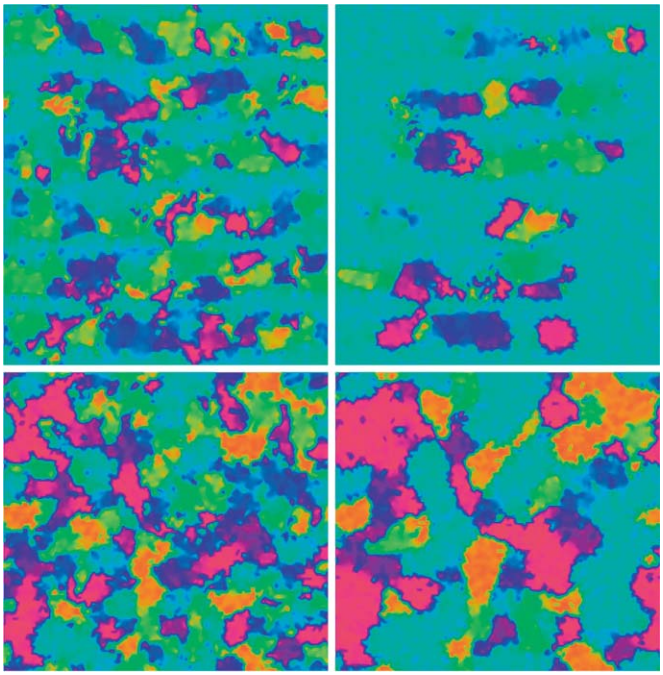

FIG. 8. Orientation distribution plots for the rectangular [1 18]-field (upper row) and the hexagonal ⟨60⟩-field (bottom row). Left and right columns correspond to evolving time, $t = 10^5$ and $t = 10^6$, respectively.

rows. These grains can be diminished by the propagating of domain layers which is a steady kinetics because the ordered region has overwhelmed predominance on these grains. However, the situation in the samples of ⟨60⟩ is very different. As the potential-well distance is as large as $6\,L_0$, which is larger than twice of the average dislocation-to-dislocation distance of about $2.5\,L_0$, these potential wells have negligible influence on the directed BCP assembly. Thus the domains around each potential well have almost independent orientation, and those domains with similar orientation will merge with each other to form larger grains, as shown by the red grains evolving from $t = 10^5$ to $10^6$. These large grains are difficult to be eliminated because their total size is comparable with that of those grains of consistent orientation with the field array. In our results, the difference of the average defect concentrations at $t = 10^5$, $(10.6 \pm 0.3)\%$ for [1 18] and $(11.5 \pm 0.5)\%$ for ⟨60⟩, is quite small. While $t = 10^6$, $(4.5 \pm 1.1)\%$ for [1 18] and $(6.9 \pm 0.5)$, the difference is increased.

Very recently, Tang and Ma studied BCP assembly on patterned templates decorated by periodic rectangularly arranged nanoposts using 2D real-space calculations of the self-consistent mean-field theory (SCFT).[32] With this equilibrium theory, they were able to observe the final equilibrium structures but the knowledge of the ordering process is lacking in the SCFT approach. These authors observe perfectly ordered cylinders/spheres under the direction of rectangular post array with as large as 34-fold density multiplication, which corresponds to $m = 17$ in the [1 m] type of rectangular field. This observation is not contradictory with our results in Fig. 7. In their model, the post array has stronger directing effect than the pure periodic field in our model because of the presence of the geometrical confinement of these posts. In addition, the equilibrium results are sensitive to the initial conditions and the iterating process when solving SCFT equations. Our results of ordering kinetics are well complementary to those from their equilibrium calculation.

## IV. CONCLUSIONS

The ordering kinetics of cylinder-forming diblock copolymer assembly under the direction of periodic rectangular fields has been studied by cell dynamics simulations of the time-dependent Ginzburg–Landau theory. A two-dimensional rectangular field, denoted as [l m], consists of potential wells with the distance of $l\sqrt{3}L_0$ along the x-direction and that of $mL_0$ along the y-direction, where $L_0$ is the cylinder-to-cylinder distance in bulk system. Our results of ordering kinetics, described by the time evolution of the defect concentration, reveal that the rectangular field of [1 m] for a given density multiplication has the best directing effect, and the reversed case of [m 1] has the worst. Compared with the case of hexagonal fields, the rectangular field has a worse directing effect for a fixed low density multiplication, however, its directing effect becomes better for a fixed high density multiplication. For example, the directing effect of the rectangular [1 8]-field is worse than that of the hexagonal ⟨40⟩-field for the density multiplication of 16. The reversed situation is that the [1 18]-field has a better directing effect than the ⟨60⟩-field for the large density multiplication of 36. The hexagonal ⟨60⟩-field has negligible effect on the directing of BCP assembly. In another word, a low-density of potential wells cannot effectively decrease grain sizes, or direct local grain orientations to be commensurate with its inherent orientation. The comparison between its evolution of defect concentration and that in uniform films indicates that the ⟨60⟩-field has little directing effect on the pattern formation. However, for the rectangular [1 18]-field, all of the potential wells are aligned in rows with a distance of $\sqrt{3}L_0$, and each row has the ability to direct layer-by-layer ordering of BCP domains. These rows restrict grain sizes along the normal direction of rows. In addition, the layer-by-layer ordering has a steady propagating speed to invade into those grains located intermediate between rows, which have mismatched orientations from the field lattice. The most important conclusion from the current study is that the rectangular pattern is alternative candidate to direct block copolymer assembly toward large-scale perfectly ordered domains in experiments.

## ACKNOWLEDGMENTS

This work is supported by the National Natural Science Foundation of China (Grants 20974026, 20704010, 20990231). W.L. gratefully acknowledges supports from the Shanghai Pujiang Program (Programs No. 08PJ1402000) and the Scientific Research Foundation for the Returned Overseas Chinese Scholars, State Education Ministry.

[1] M. Park, C. Harrison, P. M. Chaikin, R. A. Register, and D. H. Adamson, Science **276**, 1401 (1997).
[2] T. Thurn-Albrecht, J. Schotter, C. A. Kastle, N. Emley, T. Shibauchi, L. Krusin-Elbaum, K. Guarini, C. T. Black, M. T. Tuominen, and T. P. Russell, Science **290**, 2126 (2000).
[3] J. Y. Cheng, C. A. Ross, V. Z.H. Chan, E. L. Thomas, R. G.H. Lammertink, and G. J. Vancso, Adv. Mater. **13**, 1174 (2001).
[4] C. T. Black, K. W. Guarini, K. R. Milkove, S. M. Baker, T. P. Russell, and M. T. Tuominen, Appl. Phys. Lett. **79**, 409 (2001).
[5] C. Park, J. Yoon, and E. L. Thomas, Polymer **44**, 6725 (2003).
[6] F. S. Bates and G. H. Fredrickson, Annu. Rev. Phys. Chem. **41**, 525 (1990).
[7] A. Keller, E. Pedemont, and F. M. Willmout, Nature (London) **225**, 538 (1970).
[8] T. Hashimoto, J. Bodycomb, Y. Funaki, and K. Kimishima, Macromolecules **32**, 952 (1999).
[9] B. C. Berry, A. W. Bosse, J. F. Douglas, R. L. Jones, and A. Karim, Nano Lett. **7**, 2789 (2007).
[10] S. H. Kim, M. J. Misner, and T. P. Russell, Adv. Mater. **16**, 2119 (2004).
[11] T. Hashimoto, T. Ogawa, N. Sakamoto, M. Ichimiya, J. K. Kim, and C. D. Han, Polymer **39**, 1573 (1998).
[12] R. A. Segalman, H. Yokoyama, and E. J. Kramer, Adv. Mater. **13**, 1152 (2001).
[13] J. Y. Cheng, C. A. Ross, E. L. Thomas, H. I. Smith, and G. J. Vansco, Appl. Phys. Lett. **81**, 3657 (2002).
[14] J. Y. Cheng, A. M. Mayes, and C. A. Ross, Nature Mater. **3**, 823 (2004).
[15] S. O. Kim, H. H. Solak, M. P. Stoykovich, N. J. Ferrier, J. J. de Pablo, and P. F. Nealey, Nature (London) **424**, 411 (2003).
[16] M. P. StoyKovich, M. Muller, S. O. Kim, E. W. Edwards, J. J. de Pablo, and P. F. Nealey, Science **308**, 5727 (2005).
[17] R. Ruiz, H. Kang, F. A. Detcheverry, E. Dobisz, D. S. Kercher, T. R. Albrecht, J. J. de Pablo, and P. F. Nealey, Science **321**, 936 (2008).
[18] I. Bita, J. K.W. Yang, Y. S. Jung, C. A. Ross, E. L. Thomas, and K. K. Berggren, Science **321**, 939 (2008).
[19] Y. Tada, S. Akasaka, H. Yoshida, H. Hasegawa, E. Dobisz, D. Kercher, and M. Takenaka, Macromolecules **41**, 9267 (2008).
[20] Y. Tada, S. Akasaka, M. Takenaka, H. Yoshida, R. Ruiz, E. Dobisz, and H. Hasegawa, Polymer **50**, 4250 (2009).

[21]W. H. Li, F. Qiu, Y. L. Yang, and A. C. Shi, Macromolecules **43**, 1644 (2010).
[22]J. Y. Cheng, C. T. Tettner, D. P. Sanders, H. C. Kim, and W. D. Hinsberg, Adv. Mater. **20**, 3155 (2008).
[23]C. B. Tang, E. M. Lennon, G. H. Fredrickson, E. J. Kramer, and C. J. Hawker, Science **332**, 429 (2008).
[24]V. P. Chuang, J. Gwyther, R. A. Mickiewicz, I. Manners and C. A. Ross, Nano Letts. **9**, 4364 (2009).
[25]J. Xu, S. Park, S. Wang, T. P. Russel, M. O. Benjamin, and A. Checco, Adv. Mater. **22**, 2268 (2010).
[26]J. K.W. Yang, Y. S. Jung, J. B. Chang, R. A. Mickiewicz, A. Alexander-Katz, C. A. Ross, and K. K. Berggren, Nat. Nanotechnol. **5**, 256 (2010).
[27]X. M. Yang, L. Wan, S. G. Xiao, Y. Xu, and D. K. Weller, ACS Nano **3**, 1844 (2009).
[28]T. Ohta and K. Kawasaki, Macromolecules **19**, 2621 (1986).
[29]T. Ohta and A. Ito, Phys. Rev. E. **52**, 5250 (1995).
[30]M. Nonomura and T. Ohta, J. Phys.: Condens. Matter **13**, 9089 (2001).
[31]J. W. Cahn and J. E. Hilliard, J. Chem. Phys. **28**, 258 (1958) **31**, 688 (1959).
[32]Q. Y. Tang and Y. Q. Ma, Soft Matter **6**, 4460 (2010).